JACS
JOURNAL OF THE AMERICAN CHEMICAL SOCIETY
Article
pubs.acs.org/JACS

Complete Monitoring of Coherent and Incoherent Spin Flip Domains in the Recombination of Charge-Separated States of Donor-Iridium Complex-Acceptor Triads

Johannes H. Klein,[§] David Schmidt,[§] Ulrich E. Steiner,*[,‡] and Christoph Lambert*[,§]

[§]Wilhelm Conrad Röntgen Research Center for Complex Material Systems, Würzburg, Center for Nanosystems Chemistry, Institut für Organische Chemie, Universität Würzburg, Am Hubland, 97074 Würzburg, Germany

[‡]Fachbereich Chemie, Universität Konstanz 78457 Konstanz, Germany

Supporting Information

ABSTRACT: The spin chemistry of photoinduced charge-separated (CS) states of three triads comprising one or two triarylamine donors, a cyclometalated iridium complex sensitizer and a naphthalene diimide (NDI) acceptor, was investigated by transient absorption spectroscopy in the ns−μs time regime. Strong magnetic-field effects (MFE) were observed for two triads with a phenylene bridge between iridium complex sensitizer and NDI acceptor. For these triads, the lifetimes of the CS states increased from 0.6 μs at zero field to 40 μs at about 2 T. Substituting the phenylene by a biphenyl bridge causes the lifetime of the CS state at zero field to increase by more than 2 orders of magnitude (τ = 79 μs) and the MFE to disappear almost completely. The kinetic MFE was analyzed in the framework of a generalized Hayashi−Nagakura scheme describing coherent (S, $T_0 \leftrightarrow T_\pm$) as well as incoherent (S, $T_0 \rightleftharpoons T_\pm$) processes by a single rate constant $k_\pm$. The magnetic-field dependence of $k_\pm$ of the triads with phenylene bridge spans 2 orders of magnitude and exhibits a biphasic behavior characterized by a superposition of two Lorentzians. This biphasic MFE is observed for the first time and is clearly attributable to the coherent (B < 10 mT) and incoherent (10 mT < B < 2 T) domains of spin motion induced by isotropic and anisotropic hyperfine coupling. The parameters of both domains are well understood in terms of the structural properties of the two triads, including the effect of electron hopping in the triad with two donor moieties. The kinetic model also accounts for the reduction of the MFE on reducing the rate constant of charge recombination in the triad with the biphenyl bridge.

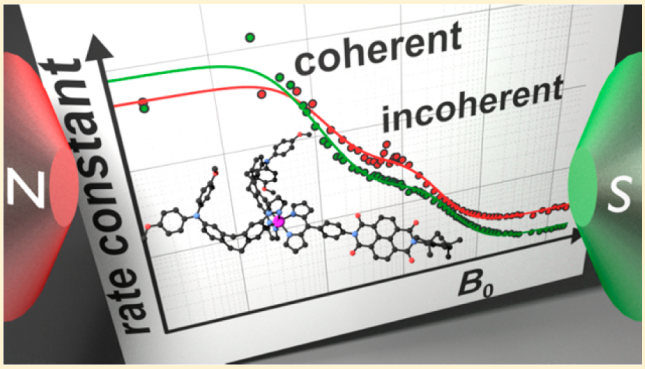

INTRODUCTION

Charge separation after light absorption and energy transfer is the first step in transforming solar energy to chemical free energy in photosynthesis.[1] This principle of photoinduced electron transfer also represents the main strategy in previous and current attempts of creating molecular systems for artificial photosynthesis by chemically linking donor and acceptor moieties. The bridge connecting donor and acceptor may also include an active chromophore supporting charge separation and/or exhibiting a sensitizer function.[2] The interest in artificial photosynthesis has provided the motivation for a vast number of investigations of chemically linked donor−bridge−acceptor systems, either with metal complex bridges[3] or pure organic spacers.[4] These studies have also proved most valuable in clarifying the fundamental laws governing the rate of electron transfer such as free energy dependence,[5] distance dependence,[6] and the transfer mechanisms of tunneling, superexchange, and hopping.[4c,6b,e−g] In this paper, we concentrate on a specific but important detail of charge recombination kinetics, i.e., the singlet−triplet equilibrium of the charge-separated (CS) states and the magnetic-field dependence caused by the spin dynamics. In particular, we provide experimental proof for a change of the spin-flip mechanism (coherent vs incoherent) which has never been observed before in such detail.

As target molecules for these investigations, we used triads **1**−**3** (Chart 1) comprising one or two triarylamine (TAA) donors, a cyclometalated iridium complex sensitizer, and a naphthalene diimide (NDI) acceptor. The TAAs were used because they have low internal reorganization energy and their oxidized form can easily be detected by optical spectroscopy.[7] The latter is also true for the NDI acceptor.[8] The dipyrrin was used as the ligand in the sensitizer because it offers several advantages over many other iridium complexes which are (i) a shift of the optical absorption down to ca. 600 nm and (ii) a ligand-centered (LC) transition in the middle of the visible spectral range much more intense than the metal-to-ligand charge transfer (MLCT) transition of many other iridium complexes absorbing in that spectral region.[9] Triad

Received: May 18, 2015
Published: June 19, 2015

DOI: 10.1021/jacs.5b04868
J. Am. Chem. Soc. 2015, 137, 11011−11021

Chart 1

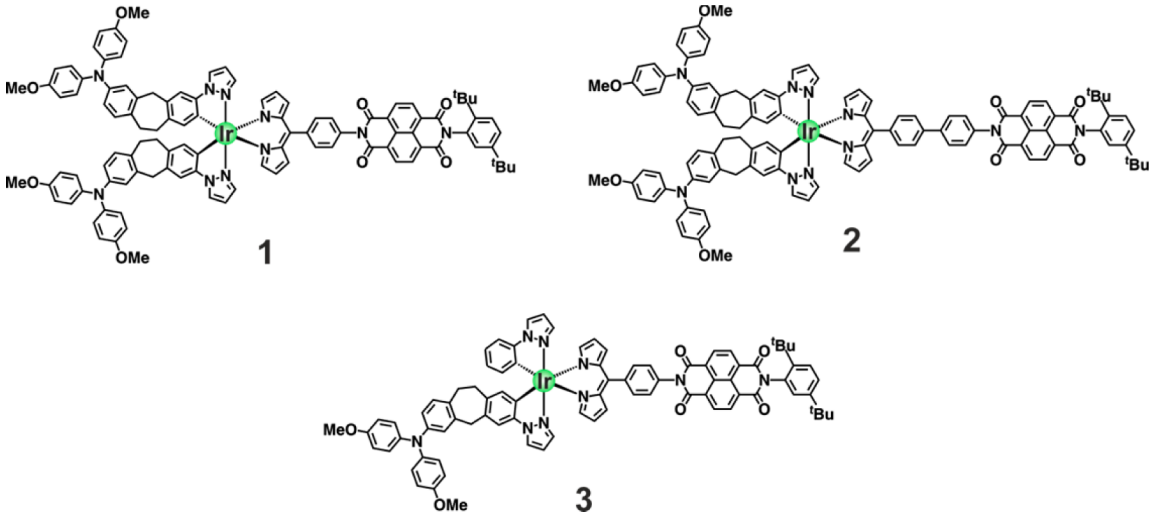

1 is known to exhibit sufficiently long-lived CS states ($\tau \approx 0.6\,\mu s$) upon irradiation and thus appears to be a suitable candidate[10] for investigating the spin dynamics of this state.[9i]

As indicated above, one of the most important aspects of CS states in linked donor–acceptor systems is related to the electron spin: these CS states represent systems with two unpaired spins, i.e., radical pairs (RPs). There are four spin configurations forming the basis of one spin state with total spin $S = 0$, a singlet state, and three spin states with $S = 1$, representing a triplet state. The substates of the latter can be distinguished according to their spin orientation in space. Due to their spatial separation, there is negligible coupling between the separate spins in triads **1**–**3**, meaning that singlet and triplet are almost degenerate. Nevertheless, their different total spins give rise to an important difference in their recombination rates, because the spin conservation rule makes recombination to a singlet ground state allowed for a singlet RP, but forbidden for a triplet RP. Conversely, if the energy of the CS state is above the energy of a locally excited triplet state, formation of such a triplet state by charge recombination is allowed for triplet RPs, but forbidden for singlet RPs.[4c,11] Therefore, any spin dynamics interconverting singlet and triplet RPs will affect the recombination rate of a RP. It is intriguing that the rates of RP spin dynamics are controlled by such weak interactions as hyperfine coupling and Zeeman interaction. This explains why the chemical decay kinetics of a RP is affected by magnetic isotope substitution patterns and by external magnetic fields. Spin chemistry[12] has moved into focus of recent interest because of its impact on optoelectronic processes in OLEDs[13] and photovoltaic devices.[14] Radical pair spin chemistry also is an essential issue in the primary processes of photosynthesis,[15] for magnetoreception[16] in animals and plants, and has found particular interest as a potential mechanism explaining the magnetic compass of migratory birds.[17]

In linked donor–bridge–acceptor systems, the spin chemistry of the CS state may be detected and characterized by the magnetic-field dependence of various observables. Transient absorption measurements represent the predominant technique, allowing to follow, e.g., the explicit time dependence of the charge recombination,[18] or the yield of triplet recombination products, if the energy of the CS state is sufficient to populate local triplets on recombination. Measurements of the latter kind have been used to detect so-called J-resonances in the magnetic-field dependence,[11c,e,f,19] allowing to determine the singlet–triplet energy separation and, hence, the extent of interaction between the unpaired electrons. Fluorescence as a very sensitive method of detection can also be utilized, if charge recombination is combined with emission, a situation typical for exciplex forming systems.[20] Finally, the spin polarization originating from the spin dynamics in the CS state can be detected using EPR methods.[4c,18g] Quite recently, a model donor–bridge–acceptor triad has been used to demonstrate that the RP spin chemistry is sensitive not only to the strength but also to the direction of the external magnetic field,[18f] thus providing a paradigm for the magnetic compass hypothesis. This particular issue has also found great interest in the field of quantum information theory.[21,22]

Before we describe our experimental findings, we briefly sum up the most important principles of RP spin chemistry. As already mentioned, the spin chemistry of RPs is characterized by the fact that chemical rate processes, such as charge recombination, are directly coupled to the conversion dynamics of the four spin substates S, T_+, T_0, and T_- (cf. Figure 1). The main interactions determining the spin conversion processes are hyperfine coupling, Zeeman interaction and exchange interaction.[4a,c,12b–d] The latter causes a splitting of the center of gravity of the triplet levels and the singlet level. It decreases exponentially with the distance between the radical centers. For

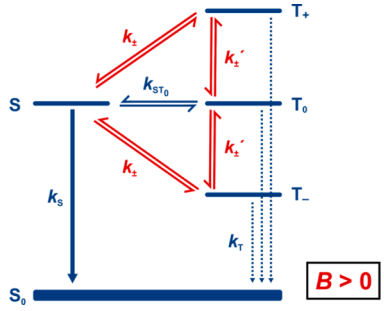

Figure 1. Reaction and spin conversion processes of a radical pair. The situation refers to a finite Zeeman splitting of the triplet levels, which vanishes at zero field, and negligible exchange interaction. The rate processes connecting the spin sublevels may be either of coherent or incoherent nature, depending on the magnitude of the Zeeman splitting in relation to the isotropic hyperfine couplings.

DOI: 10.1021/jacs.5b04868
J. Am. Chem. Soc. 2015, 137, 11011–11021

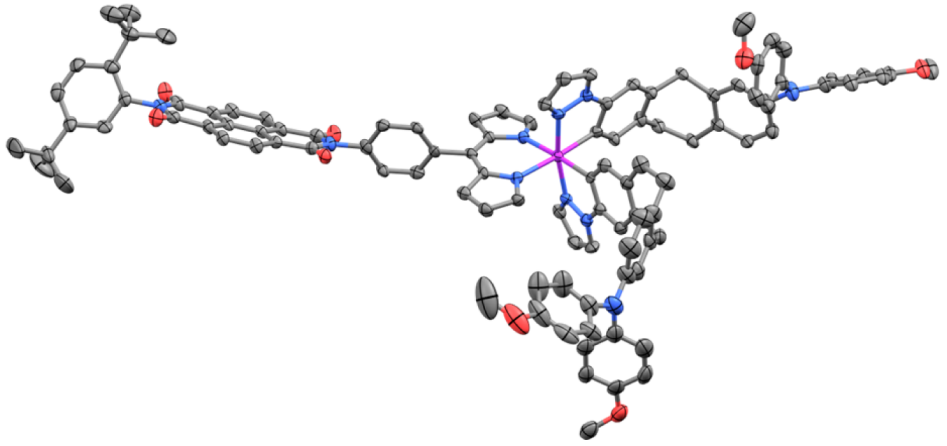

Figure 2. X-ray crystal structure of triad **1**. The ellipsoids indicate a probability level of 50%.

distances on the order of 20 Å, as applies to the triad systems investigated in this work, it is small compared to the magnitude of the hyperfine coupling and thus can be neglected.[4a,12c,d,23]

In principle, the effect of Zeeman interaction is three-fold: (i) it causes a splitting of the triplet levels and thus gradually prevents the mixing of the central substates S and T_0 with T_+ and T_- and (ii) it leads to a mixing of S and T_0 if the *g*-factors of the two radicals are different. The latter effect is insignificant in our present case because the *g*-values of organic radicals usually differ by <0.001 from the typical value of 2.0023 and very high magnetic fields are necessary to affect the spin dynamics by the Δg mechanism.[23b,f] (iii) In case of anisotropic **g**-tensors of the radicals, the Zeeman interaction is stochastically modulated by their rotational diffusion, which contributes to spin relaxation, i.e., stochastic transitions between the spin levels.[12c,24] This effect, too, is not relevant to the present work.

The by far most important interaction for organic RPs is hyperfine coupling, comprising isotropic and anisotropic contributions. If molecular rotation is sufficiently fast, the anisotropic interactions are averaged to zero. Nevertheless the short-time stochastic fluctuations of those anisotropic interactions lead to spin relaxation, albeit on a much longer time scale than molecular rotation and spin dynamics due to isotropic hyperfine interaction.[25] The latter causes a coherent process, which cannot be rigorously described by classical kinetic equations. It requires a quantum theoretical treatment of the spin density matrix of the RP by solving an appropriate Liouville equation, which comprises at the same time coherent spin motion and the stochastic decay into the chemical reaction channels.[12a,b,26] In a strict sense, quantum dynamics and chemical reaction cannot be treated separately. As mentioned above, the coherent quantum dynamics between the central and the outer Zeeman levels are more and more suppressed as the magnetic field increases. Finally, their transition rate drops below those of the incoherent transitions that are due to the modulation of anisotropic interactions and can be summarized as longitudinal (T_1-) spin-relaxation processes. In that magnetic-field regime, the description of spin transitions by rate equations is well justified. However, it must be emphasized that the transitions between S and T_0 remain coherent at any field because their Zeeman splitting remains zero. The effective rate of these processes is field independent if Δg is small, which is the case for the present systems.

In a seminal paper, Hayashi and Nagakura[27] introduced the reaction scheme shown in Figure 1 to account for the magnetic-field dependence of radical pair kinetics in the field regime where incoherent relaxation processes dominate the S, T_0 to T_+, T_- transitions and to explain the magnetic-field dependence in terms of known spin relaxation mechanisms of radicals. In the present paper, we are going to demonstrate for the investigated donor-iridium complex-acceptor triads that, formally, the kinetic scheme in Figure 1 can be applied for a wider range of magnetic fields comprising both the regime of dominant coherent and dominant incoherent spin processes. At all fields investigated, the observed decay kinetics of the RPs can be perfectly fitted using that scheme in a classical kinetics sense and treating all rate parameters as global, field independent parameters, except for $k_\pm = k_\pm'$ which depend on the magnetic field.[28] The magnetic-field dependence of $k_\pm(B)$ shows a clear transition between two regimes. We will show that in the first regime, $k_\pm(B)$ can be related to the characteristic parameters of coherent spin dynamics due to isotropic hyperfine coupling and in the second regime to the characteristics of longitudinal spin relaxation in the RP.

RESULTS

The donor-iridium complex-acceptor triads investigated in this work are shown in Chart 1. In addition to compound **1**, for which the photophysical and photochemical primary processes in the fs, ps, and ns time regimes have been characterized in detail before,[9i] the modified structures **2** and **3** were also investigated. In **2**, the phenylene group linking the iridium complex and the NDI is replaced by a biphenyl group, and **3** comprises only one triarylamine donor group. These modifications shall help to clarify structural effects on the spin chemistry of the resulting CS states.

X-ray Crystal Structure Analysis. Specific information on the molecular geometry of compound **1** was obtained by X-ray crystal structure analysis (cf. Figure 2). Single crystals of **1** were grown by liquid/liquid diffusion of hexane into a solution of **1** in dichloromethane. The structure analysis revealed a distorted octahedral iridium complex configuration with a slightly bent dipyrrin ligand. Furthermore, the dihedral angle between the phenylene ring and the neighboring NDI on the one side and the dipyrrin fragment on the other side are 121.7° and 86.1°, respectively. There are two different conformers of the TAAs relative to the iridium complex present in the solid-state structures which may also be the case in solution. The donor–acceptor distances between the center of the carbon–carbon bond of the central carbon atoms of the NDI core and the two

DOI: 10.1021/jacs.5b04868
J. Am. Chem. Soc. 2015, 137, 11011–11021

nitrogen atoms of the TAA units are 19.1 and 22.9 Å for the two possible TAA conformers.

UV−vis Spectra. The steady-state spectra of the three complexes (**1**−**3**) in MeCN are shown in Figure 3. The $\pi-\pi^*$ transition of the dipyrrin unit is observed in the visible between 15 400 and 25 000 cm^{-1} [with $\varepsilon_{max.}$(20 800 cm^{-1}) = 31 000 M^{-1} cm^{-1}].[9a−c,i] Here, the main absorption is caused by transitions to ligand-centered (LC) singlets,[9c] while the foot at ca. 17 000 cm^{-1} (588 nm) may be caused by spin-forbidden transitions to LC triplets, which gain in intensity due to the heavy-atom effect of the Ir atom. The $\pi-\pi^*$ excitations of the NDI are located between 26 600 and 31 000 cm^{-1}[29] and overlap little with the $\pi-\pi^*$ excitations of the TAA units, which absorb between 29 000 and 37 000 cm^{-1}.[9i,30] In case of complex **3**, the latter absorption is reduced due to the absence of the second TAA unit. In all three compounds, the three chromophore moieties are electronically well decoupled because of the saturated bridge between TAA and the Ir complex[9i,31] and the orbital nodes of HOMO and LUMO along the long axis of the NDI chromophore which minimizes orbital overlap to the bridging phenylene (**1** and **3**) or biphenyl (**2**) spacer.[32] In addition, both spacers show an almost 90° dihedral angle to the *meso*-position of the dipyrrin ligand (see X-ray crystal structure, Figure 2).[9b,c,i] Complexes **1** and **2** only differ by the absorption at high energy (34 000−40 000 cm^{-1}) due to the replacement of a phenylene by a biphenyl unit.

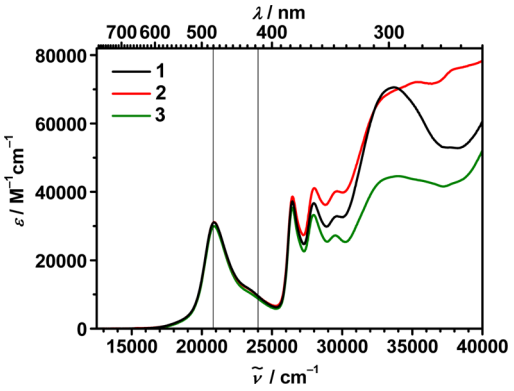

Figure 3. Absorption spectra of **1** (black), **2** (red), and **3** (green) in MeCN. The vertical lines mark laser energies 20 800 cm^{-1} (480 nm) and 24 000 cm^{-1} (416 nm) used in previous time-resolved laser experiments with compound **1** (cf. text).[9i]

Nanosecond Time-Resolved Laser-Flash Spectroscopy. Transient absorption experiments with fs- and ns-time resolution (cf. ref 9i) showed that pumping **1** in MeCN at either 20 800 or 24 000 cm^{-1} (480 or 416 nm) yields a locally excited Ir complex. After rapid (≈100 fs) intersystem crossing to the triplet, charge separation within ca. 1 ns leads to almost quantitative formation of the CS state TAA_2-[Ir(dipy)]$^+$-Ph-NDI^- (in the following to be denoted as CS_1). Further charge shift within <5 ps gives the long-lived CS state $TAA^+{}_2$-Ir(dipy)-Ph-NDI^- with a lifetime of 580 ns.[9i]

To study the spin effects in the long-lived CS states CS_2 of compounds **1**−**3**, the magnetic-field dependence of their recombination was studied using nanosecond laser-flash spectroscopy. For compound **1**, the transient Δ*OD* spectrum of CS_2 and its kinetics of formation at zero field were well characterized in ref 9i. For compound **3**, the behavior is very similar (for details cf. Supporting Information, SI).

For compound **2**, we present the pertinent observations in the following. The ns measurements of **2** at zero magnetic field were carried out in MeCN in the same way as described for **1** in ref 9i. The samples were excited with the frequency-tripled output of a Nd:YAG laser at 28 200 cm^{-1} (355 nm) shifted to 24 000 cm^{-1} (416 nm) by means of a H_2 Raman shifter. Pumping at this wavenumber produces ligand-centered excited states of the iridium complex. The transient maps were obtained by measuring the temporal decay profiles in 4 nm steps between 12 500 and 25 000 cm^{-1} (800−400 nm).

Excitation of triad **2** at 24 000 cm^{-1} (416 nm) produces a series of Δ*OD* spectra shown in Figure 4a. Starting from a strong bleaching signal, the spectra evolve to an overall positive transient spectrum. The strong bleaching signal with a minimum at ca. 20 800 cm^{-1} (480 nm) proves the initial population of ligand centered iridium complex states (see ref 9i). A kinetic trace for the rise of the signal is shown in Figure 4b. The rise time of the excited-state absorption is ca. 35 ns, which is much longer than the 0.93 ns found in the case of compound **1**[9i] and also for compound **3**. The relatively long rise time is caused by the slow charge-separation process from the triplet-excited iridium complex to the CS_1 state (see Figure S3 in the SI for the state diagram of **2**) because the ET has to proceed via the biphenyl spacer. The follow-up ET to CS_2 is fast again. The final Δ*OD* spectrum in Figure 4a shows the characteristic peaks of the TAA radical cation at 13 700 cm^{-1} (730 nm)[9i,31] and of the NDI radical anion at 21 100 and 16 600 cm^{-1} (474 and 602

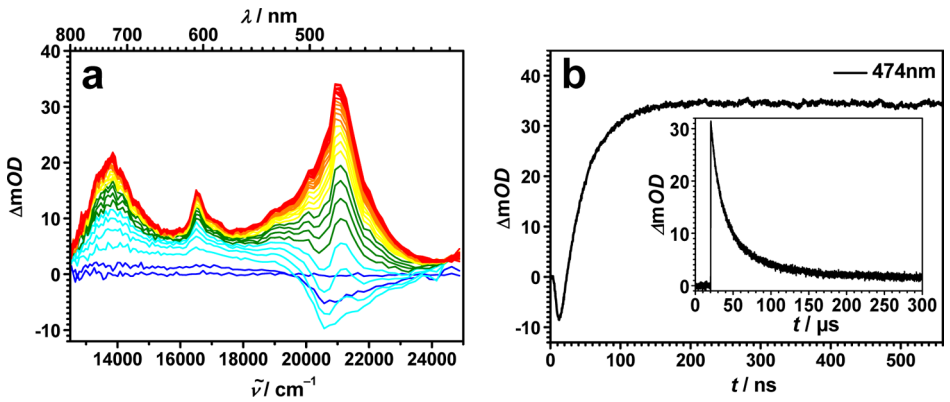

Figure 4. Transient signals observed for complex **2** under ns laser excitation at 24 000 cm^{-1} (416 nm). (a) Δ*OD* spectra in the time regime 0−162 ns: blue, 0−5.2 ns; cyan, 5.2−26.8 ns; green, 26.8−48.4 ns; yellow, 48.4−70 ns; orange, 70−97.2 ns; and red, 97.2−162 ns. (b) Decay traces at 21 100 cm^{-1} (474 nm) from transient absorption measurements with time windows of 0−540 ns and 0−300 μs (inset).

DOI: 10.1021/jacs.5b04868
J. Am. Chem. Soc. 2015, 137, 11011−11021

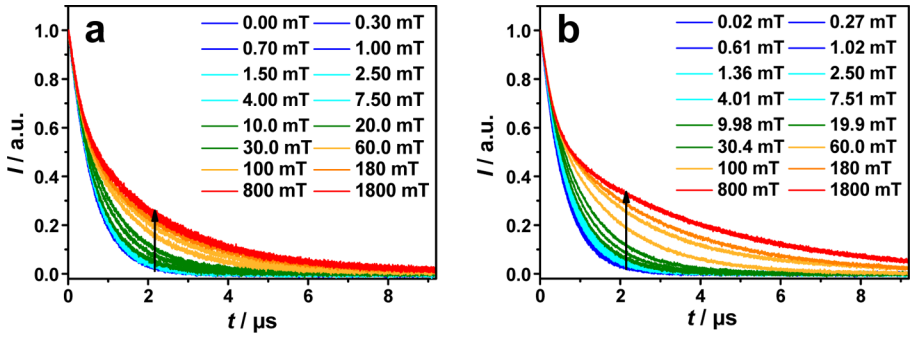

Figure 5. Selected transient absorption decay curves at 21 100 cm^{-1} (474 nm) at specified magnetic fields for complex **1** (a) and **3** (b) in MeCN. The experimental data have been normalized after correction for the finite width of the laser pulse and an offset at very long decay times (for details cf. SI).

nm)[11c,e,29a,b] which proves charge separation in **2**. Its transient spectrum decays without further changes of spectral shape (cf. Figure S6b, SI). A characteristic decay curve is shown in the inset of Figure 4b. Its decay characteristics are biexponential comprising a component of 12.3 μs (66%) and a component of 79 μs (34%).

For the observation of a second decay time, in principle two explanations may be offered: the first is the possibility of a bimolecular deactivation, which can be excluded, because the two lifetimes of the CS_2 state do not change significantly with different concentrations of 8.5×10^{-6}–4.6×10^{-5} mol L^{-1} and pulse energies of 0.2–1.0 mJ in the ns-time regime. The second explanation may be related to an additional degree of freedom of triad **2** concerning conformational changes, due to the extra phenylene ring between the NDI and the iridium complex. One can estimate that in order to observe a biphasic decay from two different excited conformers with the given amplitudes and lifetimes, the rate for interconversion of these conformers must not exceed 2000 s^{-1}. However, this appears to be much too slow for isomerization around a biphenyl axis. Thus, for the time being, we cannot offer any reasonable explanation for this observation. We emphasize, though, that both lifetimes, 12.3 and 79 μs, are exceptionally long for the recombination of a CS state in such a small triad in fluid solution at rt.

Actinometry with $Ru(bpy)_3Cl_2$ in benzene was used to measure the quantum yield of the CS state (CS_2) at 24 000 cm^{-1} (416 nm) excitation (see SI). The measurements support a very efficient ET process with a quantum yield of 97% which is as efficient as the quantum yield observed for triad **1** (almost unity).

Magnetic-Field Effects (MFE). The recombination kinetics of the CS_2 states of triads **1**–**3** were investigated for their sensitivity to an external magnetic field. For these measurements, the optical setup was changed such that the 24 000 cm^{-1} (416 nm) pump beam and the white light probe beam cross each other perpendicularly in the cavity of an electromagnet (0–1.8 T) (for details of the setup see SI). It is crucial to deoxygenate the sample solutions carefully (see SI) because MFEs are strongly reduced or not observable at all, if there are traces of O_2 in the solution.[18c,e]

The observed magnetic-field-dependent decay curves are shown in Figures 5 and 6 for a representative selection of 16 out of altogether about 50 applied magnetic fields in each case. For triads **1** and **3**, the zero-field lifetime of the CS_2 state is about 0.6 μs. In both cases, the kinetic magnetic-field effect manifests itself as a pronounced prolongation of the charge recombination process. For compound **2**, for which the zero-field lifetime of state CS_2 is on the order of 79 μs, a magnetic-field effect is hardly detectable (cf. Figure 6).

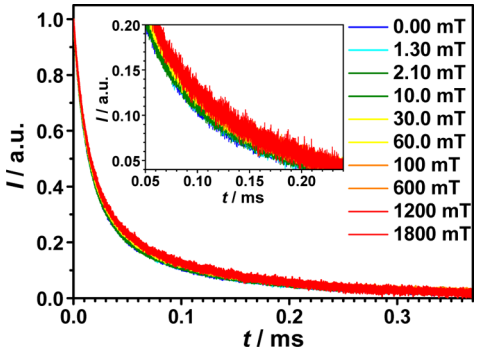

Figure 6. Experimental transient absorption decay curves for triad **2** in MeCN at various magnetic fields observed at 21 100 cm^{-1} (474 nm). The experimental data are corrected for an offset at very long decay times. Inset: Magnification of the decay curves between t = 0.05–0.24 ms.

For triads **1** and **3**, the decay curves at very low fields are monoexponential and become biexponential above about 10 mT. The field effects saturate above 800 mT, reaching a longer lifetime component of 2.2 μs for triad **1** and 3.9 μs for triad **3**, corresponding to 3.8- and 6.6-fold increases, respectively, relative to zero field. Half of the maximum lifetime effects are reached around 50–60 mT.

Kinetic Model of Magnetic Field-Dependent Charge Recombination. As a generic basis of our kinetic simulation we will use the reaction scheme given in Figure 1. As was shown by Hayashi and Nagakura, this scheme is an appropriate description of RP reaction dynamics if the spin processes between the central Zeeman levels S and T_0 and the outer Zeeman levels T_+ and T_- are due to relaxation, i.e., incoherent processes, and the S/T_0 equilibration can be considered as being fast.[27] In a more general phenomenological approach, we assume that the scheme also applies to the situation where coherent spin processes participate in the interconversion of the four spin substates. In setting up the kinetic equations, we take $k_{\pm} = k_{\pm}'$ which is correct if spin processes induced by electron spin dipolar interaction can be neglected, which, like the vanishing exchange interaction, should be a reasonable assumption for spin–spin separations on the order of 20 Å.[33] Due to the symmetry of the parameter pattern, T_+ and T_- will behave exactly identically. Then, the kinetic equations following from the reaction scheme in Figure 1 are[34]

DOI: 10.1021/jacs.5b04868
J. Am. Chem. Soc. 2015, 137, 11011–11021

$$
\begin{aligned}
d[S]/dt &= -(k_S + 2k_\pm + k_{ST_0})[S] + k_{ST_0}[T_0] + k_\pm([T_+] + [T_-])\\
d[T_0]/dt &= k_{ST_0}[S] - (k_T + 2k_\pm + k_{ST_0})[T_0] + k_\pm([T_+] + [T_-]\\
d[T_+]/dt &= k_\pm[S] + k_\pm[T_0] - (k_T + 2k_\pm)[T_+]\\
d[T_-]/dt &= k_\pm[S] + k_\pm[T_0] - (k_T + 2k_\pm)[T_-]
\end{aligned}
\tag{1}
$$

The general solution of this system of linear differential equations is a triexponential function. Although a general analytical expression could be given, it is very clumsy. Instead, solutions for concrete parameter values were calculated by MATHEMATICA, yielding the numerical values of the coefficients and time constants of the exponentials. Plain tabular numerical solutions were also obtained using MatLab. The experimentally observed decay curve represents the superposition of the concentrations of all spin substates of the CS_2 state.

Fit Strategy and Evaluation of Global Parameters. Before fitting the CS_2 decay signals, these were standardized (i) by correcting the initial part for the pulse width of the laser and the finite response time of the detection system (for details cf. SI), (ii) by subtracting a small long-time offset showing at the end of the signals, and (iii) by normalizing the corrected signal amplitude to 1.

With regard to the kinetic parameters in eq 1, we note that the rate constants k_{ST_0}, k_S, and k_T must be considered as independent of the magnetic field. The same applies to the initial spin configuration, to be specified by the singlet probability p_S. Thus, for a series of signals measured for each of the triads under various magnetic fields, these parameters must be treated as global constants for each triad, and the only parameter varying with the field is rate constant $k_\pm$. The problem of fixing the global parameters is simplified by the fact that it seems safe to assume that $k_T \approx 0$,[18d] because no strong spin−orbit coupling effects are to be expected for the two organic radical moieties in the vicinity of a diamagnetic iridium core.

For the determination of a physically significant value of the rate constant k_{ST_0}, we resort to the semiclassical model of Schulten and co-workers[35] for the coherent hyperfine-driven motion of the electron spins in a radical pair. In this model, the hyperfine coupling constants a_{ik} for the individual radicals sum up to a classical vector by $I_i = \sum_k a_{ik} I_{ik}$ and are given as follows: for NDI[36] $2 \times \alpha_N = 0.095$ mT, $4 \times \alpha_H = 0.190$ mT; for TAA[6d] $4 \times \alpha_H = 0.055$ mT, $4 \times \alpha_H = 0.203$ mT, $6 \times \alpha_H = 0.084$ mT, $2 \times \alpha_H = 0.160$ mT, $2 \times \alpha_H = 0.094$ mT, $1 \times \alpha_N = 0.921$ mT, $1 \times \alpha_H = 0.210$ mT. According to Schulten and Wolynes,[35a] the evolution of spin character based on these values is obtained as shown in Figure 7 for zero field and (infinitely) high field.

In order to apply the classical kinetic rate eqs 1 we need to approximate the spin evolution of the Schulten−Wolynes model by classical kinetic equations. To achieve this, we describe the approach to spin-equilibrium using the kinetic model in eq 1. For convenience, we start from a pure triplet. In this case, the general result for the evolution of singlet character is

$$
p_S(t) = \frac{1}{4}\left(1 - \frac{1}{3}e^{-4k_\pm t} - \frac{2}{3}e^{-2(k_{ST_0}+k_\pm)t}\right) \tag{2}
$$

In the limit of zero field, it can be assumed that $k_\pm \approx k_{ST_0}$ yielding

$$
p_{S,zf}(t) = \frac{1}{4}(1 - e^{-4k_{ST_0}t}) \tag{3}
$$

In the high-field case, $k_\pm \to 0$, yielding

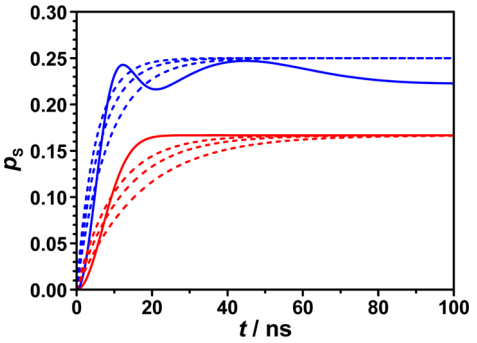

Figure 7. Evolution of singlet probability p_S in a CS_2 state starting from a pure triplet spin configuration. Solid lines (blue, zero field; red, high field) calculated according to the semiclassical model by Schulten and Wolynes.[35a] Dashed lines from top to bottom represent classical kinetic behavior according to eqs 3 and 4, with $k_{ST_0} = 5 \times 10^7$, 4×10^7, and 3×10^7 s^{-1} blue, zero field; red, high-field approximation. For details cf. text.

$$
p_{S,hf}(t) = \frac{1}{6}(1 - e^{-2k_{ST_0}t}) \tag{4}
$$

In Figure 7, the pertinent classical kinetics of zero- and high-field curves are shown for $k_{ST_0} = 3 \times 10^7$, 4×10^7, and 5×10^7 s^{-1}, three representative values of k_{ST_0}, for which the obtained kinetics define a range wherein a sensible approximation must be sought. Adopting the two extremes of these values, the global best fit for k_S was determined for a series of trial values for p_S (for details cf. SI). It turned out that for both limiting trial values of k_{ST_0} the global root mean square (rms) minimum was centered around an initial singlet population of $p_{S,0} = 0.25$, i.e., full equilibrium between the spin substates of the RP. To proceed further, we adopted a k_{ST_0} value of 4×10^7 s^{-1}, i.e., central to the two examined border cases shown in Figure 7. Values of $k_S = 6.7 \times 10^6$ s^{-1} for triad **1** and 6.97×10^6 s^{-1} for triad **3** were obtained as global minima for $p_{S,0} = 0.25$ and $k_{ST_0} = 4 \times 10^7$ s^{-1}.

To fix the best $k_\pm$ values for the individual decay curves, consistent fits were performed with MatLab and MATHEMATICA. The procedure to obtain the $k_\pm$ value with minimum rms deviation and the error bounds of $k_\pm$ for each field is demonstrated in Figure 8. It must be emphasized that the variation of the single parameter $k_\pm$ was sufficient to obtain excellent fits of the decay curves for all fields. The resulting field dependences of $k_\pm$ for triad **1** and **3** are shown in Figure 9. For both compounds, the magnetic-field dependence of the $k_\pm$ values could be fitted by a double Lorentzian according to eq 5 using the parameters listed in Table 1.

$$
k_\pm(B) = \frac{k_{hfc,0}}{1 + (B/B_{1/2,hfc})^2} + \frac{k_{rel,0}}{1 + (B/B_{1/2,rel})^2} + k_{rel,\infty} \tag{5}
$$

DISCUSSION

Initial Spin Population. When fitting the $k_\pm$ values, $p_{S,0} = 0.25$, i.e., initial spin equilibrium, had to be assumed, because it represents the best global value for all fields. The physical reason for this instance lies in the nature of the RP CS_1, the precursor state of RP CS_2. CS_1 corresponds to the CS state TAA_2-$[Ir(dipy)]^+$-Ph-NDI^-,[9i] where an unpaired electron spin is situated at the iridium core which is in a formal Ir^{4+} oxidation state with a d^5 electron configuration. As is well-known from Ru

DOI: 10.1021/jacs.5b04868
J. Am. Chem. Soc. 2015, 137, 11011−11021

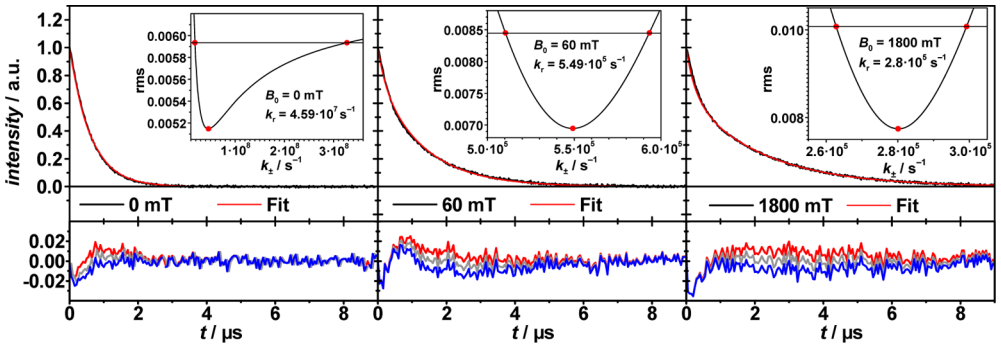

Figure 8. Demonstration of procedure and accuracy of fitting $k_\pm$ as a function of magnetic field, here 0, 60, and 1800 mT. Top: observed decay curve in black and fitted curve in red. Bottom: residual plot of difference between observed and fitted decay curve. Gray, best fit; and red and blue, using $k_\pm$ values yielding residuals about one noise width apart. Inset: rms deviation as a function of $k_\pm$ with indication of minimum and error bounds within the signal noise width. The pertinent best fit $k_\pm$ values are indicated in the inset diagrams (for more details cf. SI).

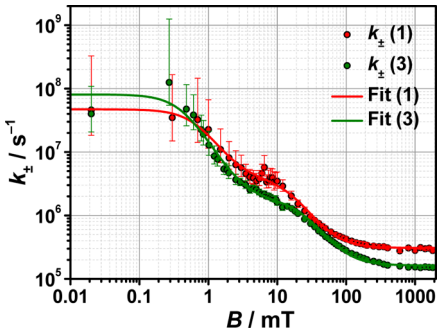

Figure 9. Magnetic-field dependence of $k_\pm$ with error bars obtained by fitting the CS_2 decay curves as illustrated in Figure 8. Red, triad **1**; and green, triad **3**. The solid lines represent best fits of the double Lorentzian function of eq 5 to the data. The parameters are given in Table 1.

and Fe spin chemistry,[37,38] the d^5 complexes of these elements show extremely short spin relaxation times on the order of a few ps, which are due to an efficient Orbach mechanism based on the small energy gap between the ground and the first excited doublet state. In RPs involving such species the spin equilibrium is also obtained within a few ps. The analogous situation can be anticipated for Ir.

Error Bars. As shown in Figure 9, for triads **1** and **3** the magnetic-field dependence of the rate parameter $k_\pm$ is very well-defined over 2−3 orders of magnitude. For triad **3**, the error bars become large only at magnetic fields below 1 mT, for triad **1**, below 10 mT. The larger error bars at low fields are due to the fact that for high values of $k_\pm$ the decay kinetics get less sensitive to this parameter, since the substate populations of the RP remain close to spin statistical equilibrium. This circumstance is also responsible for the fact that the error bars become asymmetric with a longer upper part. However, in spite of some uncertainties of $k_\pm$ at low fields, the density of data points down to 0.4 mT is high enough to provide a convincing basis for defining the double Lorentzian fit, which, as will be shown, represent the two kinetic regimes of coherent and incoherent transitions between the central and the outer Zeeman levels of the RP.

The Regime of Coherent Spin Flips. While Lorentzian line shapes are well founded in relaxation theory, where they represent the energy dependence of spectral densities of stochastic perturbations,[24,39] their use to describe the magnetic-field dependence of coherent spin processes or product yields depending on such processes has not been customary in the literature. Nevertheless, from a formal phenomenological point of view, the Lorentzian function is quite suitable to describe such cases, too. Examples from the literature[40,18b] are given in the SI. As a qualitative rationale of such applications, one may refer to the inverse energy dependence of mixing coefficients according to first order perturbation theory and the proportionality of reaction probabilities to the square of mixing coefficients. Quantitative studies with freely diffusing radical pairs have furnished the following approximate relation between the hyperfine coupling constants of the radicals and the $B_{1/2}$ field of the magnetic effect of spin-selective recombination yields[12c,19]

$$B_{1/2} = \sqrt{3(B_1^2 + B_2^2)} \tag{6}$$

with the individual B_i given by the following sum over the nuclei k in either radical,

$$B_i = \sqrt{\sum_k a_{ik}^2 I_{ik}(I_{ik} + 1)} \tag{7}$$

a_{ik} representing the isotropic hyperfine coupling constant of nucleus k in radical i. From the hyperfine coupling constants of the CS_2 radical moieties given in the Results section, a $B_{1/2}$ value of 2.5 mT is obtained for all three triads. The $B_{1/2}$ values found by the Lorentzian fit of the low-field branch of the dependence of $k_\pm$ on the magnetic field B, viz. 0.69 mT for triad **1** and 0.44 mT for triad **3**, are significantly smaller. However, one must note that relations as given in eq 6 result from convolutions of spin evolution and re-encounter probabilities, the latter usually decaying on the time scale of a few nanoseconds. On the other hand, we are dealing here with linked radical pairs, recombining in spin-allowed transitions on the time scale of several hundreds of nanoseconds. On such time-scales, smaller magnetic fields are sufficient to achieve the same effect as higher fields on the few-

Table 1. Fit Parameters of the Curves Fitting $k_\pm(B)$ in Figure 9 According to Eq 5

	$k_{hfc,0}$ (s^{-1})	$B_{1/2,hfc}$ (mT)	$k_{rel,0}$ (s^{-1})	$B_{1/2,rel}$ (mT)	$k_{rel,\infty}$ (s^{-1})
triad **1**	$(4.3 \pm 0.4) \times 10^7$	0.69 ± 0.07	$(3.6 \pm 0.25) \times 10^6$	15 ± 1	$(3.1 \pm 0.1) \times 10^5$
triad **3**	$(7.9 \pm 1.1) \times 10^7$	0.44 ± 0.04	$(1.6 \pm 0.1) \times 10^6$	25 ± 2	$(1.64 \pm 0.08) \times 10^5$

DOI: 10.1021/jacs.5b04868
J. Am. Chem. Soc. 2015, 137, 11011−11021

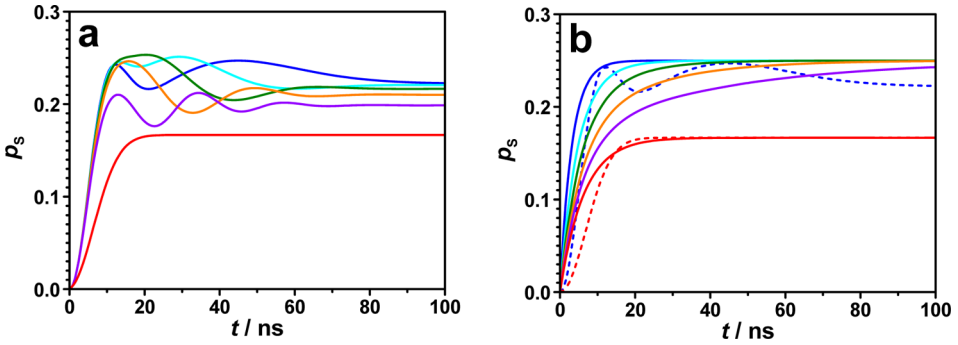

Figure 10. Establishment of spin equilibrium represented as time evolution of singlet character when starting with a pure triplet RP. (a) Results for semiclassical model:[35] blue, 0 mT; cyan, 0.44 mT; green, 0.7 mT; orange, 1.0 mT; purple, 1.5 mT; red, high-field limit. (b) Results for classical model according to eq 2 with $k_{\pm}$ values according to the first Lorentzian function in eq 5 and k_{ST_0} given by the parameter $k_{hfc,0}$ for triad **3** in Table 1. For comparison, the limiting zero-field and high-field cases in the semiclassical mode are shown as dashed lines.

nanosecond time scale. A comparison of spin-equilibration kinetics using the semiclassical approach[35] in Figure 10a and the classical kinetic approach in Figure 10b may be illuminating. Although, in principle, the oscillatory behavior peculiar to the coherent dynamics cannot be reproduced by the classical monoexponential kinetics, it is borne out by the two sets of curves that the magnetic field affects the spin population on the same overall time scale. Thus, it appears out of doubt that the first branch of the double Lorentzian in Figure 9 does indeed account for the coherent transitions between the central and the outer Zeeman levels of the RP. A rigorous theoretical transformation of the coherent picture of spin dynamics to the equivalent classical representation is only possible by solving the pertinent stochastic Liouville equation of the full quantum theoretical problem including spin dynamics and spin-selective chemical reaction simultaneously. This will be subject to future work.

Interestingly, in spite of the identical hyperfine coupling situation, the $B_{1/2}$ value of triad **1** is significantly larger than that of triad **3**. The structural property to which this difference may be assigned is the second triarylamine donor group attached to the central complex in triad **1**. Energetically, it does not make a difference which of the two donor groups donates the electron, but once one of them has been oxidized, the possibility of degenerate hole exchange between the two TAAs arises. Such a process limits the time period of unperturbed spin evolution due to the hyperfine coupling at the oxidized site. It has been shown[35b,41] that degenerate electron exchange leads to a broadening of the observed magnetic-field dependence with the approximate relation:

$$k_{exch} \approx \gamma_e \Delta B_{1/2} \tag{8}$$

with γ_e the gyromagnetic ratio of the electron. Interpreting the difference of 0.25 mT between the $B_{1/2,hfc}$ values of triad **3** and **1** by eq 8, we estimate $k_{exch} \approx 4.4 \times 10^7$ s^{-1}. This order of magnitude is in excellent agreement with recent results from EPR measurements on intramolecular hole exchange in organic mixed-valence compounds based on symmetric bis-(triarylamine)paracyclophane redox systems with similar electron hopping distances as in the present case.[42] In contrast, in a recently published donor-iridium dipyrrin-acceptor triad, where the triarylamine donors are directly attached to the phenylpyrazole framework of the iridium complex, the coupling between the oxidized and the neutral TAA via the iridium d orbital is so strong that this interaction is manifested by an intervalence charge-transfer band in the NIR spectral region.[43]

Thus, we see that the magnetic-field dependence of the first Lorentzian branch carries quite specific information on the systems investigated. Also in line with the explanation by electron exchange is the fact that in case of triad **1**, the field dependence extrapolates to lower values at zero field ($k_{hfc,0}$) than in case of triad **3**. Shortening the time available for coherent spin evolution by electron hopping will also decrease the T ⇌ S transition rates.

Although our present findings seem to be the first clear demonstration of the region of coherent hyperfine-induced S ⇌ T transitions using classical kinetics, we note that in previous work, involving one of the present authors, on donor−acceptor systems linked through a $Ru(bpy)_3^{2+}$ complex[18c] there was an indication, albeit unnoticed in that work, of the analogous situation. The data referring to the equivalent of the present rate constant $k_{\pm}$, dubbed k_r in ref 18c because it was meant to be entirely due to relaxation, were sparser than in the present case, and a point of inflection was not apparent. But the field range of change of this parameter k_r was too extended to be fitted by a single Lorentzian. Thus, two Lorentzians were used, with "correlation times" of 2 and 0.25 ns. In our present view, the longer correlation time corresponds to a $B_{1/2}$ of 2.8 mT which exactly matches the theoretical $B_{1/2}$ calculated from the hyperfine coupling constants of that system using eq 6.

The Regime of Incoherent Spin Flips at 10 mT < *B* < 1 T. The second Lorentzian component in the magnetic-field dependence of $k_{\pm}$ must be assigned to incoherent spin relaxation processes in the individual radicals. As shown in the SI, from the longitudinal relaxation time T_1 of any of the radicals, the following contribution to $k_{\pm}$, to be denoted k_{rel} in the Lorentzian domain assigned to spin relaxation, is derived

$$k_{rel}(T_1) = \frac{1}{4T_1} \tag{9}$$

Since **g**-tensor anisotropies are small and the distance between the radical moieties is too large for electron-spin dipolar interaction to become effective, the major mechanistic contribution to spin relaxation of the radical species involved in the CS_2 states should be due to the rotational modulation of anisotropic hyperfine coupling. The dominating hyperfine interaction is due to the ^{14}N nucleus of the triarylamine radical moiety. For negligible **g**-tensor anisotropy the transversal relaxation time is given by[44]

$$\frac{1}{T_1} = \frac{2}{9} I(I+1) \sum_i (A_{ii} - A_{iso})^2 \frac{\tau_c}{1 + \omega_0^2 \tau_c^2} \tag{10}$$

DOI: 10.1021/jacs.5b04868
J. Am. Chem. Soc. 2015, 137, 11011−11021

For axial symmetry, this expression can be transformed to

$$\frac{1}{T_1} = \frac{4}{27} I(I+1)\Delta A^2 \frac{\tau_c}{1+\omega_0^2\tau_c^2} \quad (11)$$

where the hyperfine coupling anisotropy

$$\Delta A = A_{\parallel} - A_{\perp} \quad (12)$$

is given in angular frequency units. The quantities I, ω_0, and τ_c represent total nuclear angular momentum quantum number, Larmor frequency, and rotational correlation time, respectively.

Combining eqs 9 and 11 and substituting $I = 1$ for a ^{14}N nucleus yields

$$k_{rel} = \frac{2}{27}\Delta A^2 \frac{\tau_c}{1+\omega_0^2\tau_c^2} \quad (13)$$

Relating the parameters in eq 13 to the fit parameters $k_{rel,0} = 3.6 \times 10^6$ s^{-1} and $B_{1/2,rel} = 15$ mT for triad **1** and $k_{rel,0} = 1.6 \times 10^6$ s^{-1} and $B_{1/2,rel} = 25$ mT for triad **3** yields $\Delta A = 3.6 \times 10^8$ rad·s^{-1} (2.0 mT) and $\tau_c = 0.38$ ns for triad **1** and $\Delta A = 3.1 \times 10^8$ rad·s^{-1} (1.75 mT) and $\tau_c = 0.23$ ns for triad **3**. To estimate the rotational correlation times on the basis of the Einstein−Debye equation

$$\tau_c = \frac{4\pi R^3}{3kT}\eta \quad (14)$$

we substitute 0.343 mPa·s for the solvent viscosity η of MeCN and the values 10.6 and 9.54 Å (cf. SI) for the hydrodynamic radii of triads **1** and **3**, respectively, yielding 0.42 ns for triad **1** and 0.30 ns for triad **3** in fairly good agreement with the correlation times from the Lorentzian fits.

Directly applicable literature data on the anisotropy of hyperfine coupling ΔA of the N atom in the present triarylamine radical moieties are not available, but quantum chemical calculations for phenoxazine radicals[45] and for its sulfur and selenium heteroanalogues have shown that the anisotropy ΔA of hyperfine coupling of the ^{14}N atom is about 2.7 times its isotropic value, which indicates that it results mainly from the dipolar interaction between the nuclear spin and the electron spin in the 2p orbital and only a small part of the isotropic hyperfine interaction is due to spin polarization of the 2s orbital. About the same ratio is obtained for the inorganic radicals $N(SO_3)_2^{2-}$ and $NH(SO_3)^-$.[39] If we assume the same relationship to hold for the present triarylamine radical, ΔA would be on the order of 2.7 × 0.92 mT ≈ 2.5 mT. The observed values are not far off, indeed.

The Regime of Incoherent Spin Flips at $B > 1$ T. The magnetic-field-independent contributions $k_{rel,\infty}$ to the rate constants $k_{\pm}$ were found to be 3.1×10^5 s^{-1} for triad **1** and 1.64×10^5 s^{-1} for triad **3**. These values are on the same order of magnitude as the value of 5×10^5 s^{-1} reported for a radical pair constituted by the diquat monoradical cation and the oxazin radical cation.[45] Spin-rotational coupling as a magnetic field independent mechanism of spin relaxation may be discarded for that as well as the present cases because in the systems under consideration the spin−orbit coupling effects are small as indicated by **g**-tensor values close to that of a free electron. Apparently, only a "local mode" mechanism that modulates spin−orbit coupling can be held responsible here as was also postulated in case of trityl radicals.[46] Systematic studies of structural variations affecting this mechanism, however, do not seem to be available in the literature.

The MFE in Triad 2. Our discussion of the behavior of triads **1** and **3** has shown that their magnetic-field-dependent kinetics represent a rich source of information on the internal spin dynamics of the CS states. However, for triad **2**, magnetic-field effects are hardly observable. This goes along with the fact that in this case the recombination of the CS_2 state is about a factor of 100 slower than for triads **1** and **3**. It takes place on the time scale of about 100 μs, while in the former cases, it is completed in <10 μs at zero field. This lifetime effect is clearly a consequence of the longer separation of the acceptor part by a biphenyl bridge. Furthermore, also distinct from triads **1** and **3**, for triad **2** the decay is biexponential even at zero field. Such a behavior is not explicable in terms of spin dynamics, which is expected to occur at the same rate as in the other two cases, so that on the 10−200 μs time scale spin equilibrium should be always established and the four spin states should decay as one kinetic quasi species. Thus, the biexponential decay at zero field can be only assigned to the decay of two distinct species CS_2 and CS_2' that are not in rapid equilibrium. In Figure 11, the biexponential decomposition

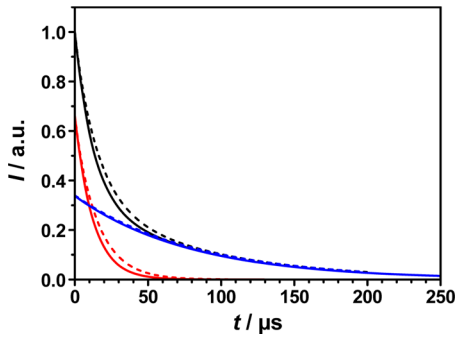

Figure 11. Prediction of magnetic-field effect for triad **2**. Black solid line: simulation of observed decay curve at zero field by a superposition of two exponentials shown separately as red and blue solid curves. Dashed curves: estimated magnetic-field effects for high fields, assuming $k_{rel,\infty} = 10^5$ s^{-1}. For details cf. text.

is shown, which is characterized by the amplitudes 0.66 and 0.34 and the decay constants 8.12×10^4 and 1.26×10^4 s^{-1}, respectively. Assuming that in each species, CS_2 and CS_2', the rate constants k_{ST_0} and $k_{\pm}$ correspond to those of triads **1** and **3** and that we start with spin equilibrium ($p_S = 0.25$) at $t = 0$, fitting each of the exponentials in Figure 11 yields k_S values of 3.2×10^5 and 5.0×10^4 s^{-1} for the CS_2 species with the faster and the slower decaying exponential, respectively. With all these parameters fixed, we can estimate the maximum expectable magnetic-field effect at high fields, by setting $k_{rel,\infty} = 10^5$ s^{-1}, i.e., the same order of magnitude as observed for triads **1** and **3**. The resulting decay curves are shown as dashed lines in Figure 11. They are in good agreement with the experimental observations (see Figure 7). This shows that, just by reducing the recombination rate k_S, the magnetic-field sensitivity is greatly reduced. What is still not clear at present is the structural nature of the two modifications of CS_2 in case of triad **2**. Several conceivable possibilities have been already rejected in the Results section. Another obvious explanation might be the inequivalence of the two donor groups (cf. structure in Figure 2). However, if the electron hopping rate of about 5×10^7 s^{-1}, deduced from the $B_{1/2,hfc}$ shift of the low-field Lorentzian between triads **1** and **3**, is realistic, then the two donor sites cannot exhibit different kinetics on the time-scale of 100 μs, because the exchange is too rapid.

CONCLUSIONS

The present work investigates the spin chemistry of three structurally related rigid donor-iridium complex-acceptor triads

DOI: 10.1021/jacs.5b04868
J. Am. Chem. Soc. 2015, 137, 11011−11021

by means of a MFE on the recombination kinetics and reveals a number of remarkable novel features. Over the full magnetic field range from 0 to 2 T, the observed kinetic MFE could experimentally be resolved in unprecedented detail and consistently be reproduced by an extended version of the Hayashi−Nagakura scheme. We have shown that this scheme is not only suitable to simulate the incoherent T_1-type spin relaxation processes at higher fields but also that a single, magnetic-field-dependent rate constant $k_{\pm}(B)$ can be used to account for coherent S, $T_0 \leftrightarrow T_{\pm}$ mixing at low fields. Phenomenologically, the full field dependence of $k_{\pm}$ can be decomposed into two clearly separated Lorentzian branches. The parameters of the low-field branch ($k_{hfc,0}$ and $B_{1/2,hfc}$) can be related to the coherent spin motion driven by isotropic hyperfine coupling and reveal quantitative information even on such fine details as the presence of degenerate electron exchange between the two donor moieties in triad **1**, which becomes evident from the comparison with triad **3**, comprising only one donor. In contrast, the high-field Lorentzian branch is due to T_1 spin relaxation, driven by rotational modulation of anisotropic hyperfine coupling, whereby the $B_{1/2,rel}$ values clearly indicate the molecular radius effect on the rotational correlation time. In addition, the very weak kinetic MFE of triad **2**, containing a biphenyl linker between complex and acceptor part, is consistently accounted for by the spin chemical kinetic scheme. Since the longer biphenyl linker slows down the back electron transfer by more than 2 orders of magnitude, this process becomes too slow to be an efficient monitor of the magnetic-field dependence of the much faster spin processes. Thus, our interpretation of the first clearly observed biphasic, double Lorentzian spin-flip characteristics are well supported and open up important new insight into the details of molecular motion, spin interconversions, and chemical rate processes of the CS states of metal-complex-sensitized triads.

The small $B_{1/2,hfc}$ values for triad **1** (0.69 mT) and for triad **3** (0.44 mT) characterizing the coherent spin-flip process are about 1 order of magnitude larger than the earth magnetic field (0.048 mT). Modifying one or two spin bearing units in order to decrease the effective magnetic moment (see eq 7) thus seems to be a viable way to construct artificial systems that are sensitive to the earth magnetic field and to mimic magnetoreceptors, as they might be involved, e.g., in the avian magnetic compass of birds, specifically studied in refs 18f, g, 26, and 47.

■ ASSOCIATED CONTENT

Supporting Information

Synthesis, single-crystal structure analysis, cyclic voltammetry, transient absorption spectra and global analysis data, spin chemical equations, and global fitting procedure. The Supporting Information is available free of charge on the ACS Publications website at DOI: 10.1021/jacs.5b04868.

■ AUTHOR INFORMATION

Corresponding Authors

*ulrich.steiner@uni-konstanz.de

*christoph.lambert@uni-wuerzburg.de

Notes

The authors declare no competing financial interest.

■ ACKNOWLEDGMENTS

The group at Würzburg acknowledges generous support within the collaborative research project "Solar Technologies Go Hybrid" by the Bavarian State Ministry for Science, Research and the Arts, support from the EU COST-Action "Perspect H_2O" as well as from the Deutsche Forschungsgemeinschaft (GRK 2112). Furthermore, we would like to thank Alexander Schmiedel and Dr. Marco Holzapfel for the measurement and analysis of the fs pump−probe measurements of triad **2** (see SI).

■ REFERENCES

(1) Hall, D. O.; Rao, K. K. *Photosynthesis*; Cambridge University Press: Boca Raton, FL, 1994.

(2) (a) Kodis, G.; Lidell, P. A.; Moore, A. L.; Moore, T. A.; Gust, D. *J. Phys. Org. Chem.* **2004**, *17*, 724. (b) Tachibana, Y.; Vayssieres, L.; Durrant, J. R. *Nat. Photonics* **2012**, *6*, 511. (c) McConnell, I.; Li, G.; Brudvig, G. W. *Chem. Biol.* **2014**, *17*, 434.

(3) (a) Wenger, O. S. *Coord. Chem. Rev.* **2009**, *253*, 1439. (b) Flamigni, L.; Collin, J. P.; Sauvage, J. P. *Acc. Chem. Res.* **2008**, *41*, 857. (c) Magnuson, A.; Anderlund, M.; Johansson, O.; Lindblad, P.; Lomoth, R.; Polivka, T.; Ott, S.; Stensjo, K.; Styring, S.; Sundstrom, V.; Hammarstrom, L. *Acc. Chem. Res.* **2009**, *42*, 1899. (d) Baranoff, E.; Collin, J. P.; Flamigni, L.; Sauvage, J. P. *Chem. Soc. Rev.* **2004**, *33*, 147. (e) Balzani, V.; Credi, A.; Venturi, M. *ChemSusChem* **2008**, *1*, 26.

(4) (a) Verhoeven, J. W. *J. Photochem. Photobiol. C* **2006**, *7*, 40. (b) Wasielewski, M. R. *Chem. Rev.* **1992**, *92*, 435. (c) Wasielewski, M. R. *J. Org. Chem.* **2006**, *71*, 5051.

(5) (a) Marcus, R. A. *J. Chem. Phys.* **1955**, *24*, 966. (b) Miller, J. R.; Calcaterra, L. T.; Closs, G. L. *J. Am. Chem. Soc.* **1984**, *106*, 3047.

(6) (a) Closs, G. L.; Calcaterra, L. T.; Green, N. J.; Penfield, K. W.; Miller, J. R. *J. Phys. Chem.* **1986**, *90*, 3673. (b) Paddon-Row, M. N. *Aust. J. Chem.* **2003**, *56*, 729. (c) Edwards, P. P.; Gray, H. B.; Lodge, M. T. J.; Williams, R. J. P. *Angew. Chem., Int. Ed.* **2008**, *47*, 6758. (d) Kattnig, D. R.; Mladenova, B.; Grampp, G.; Kaiser, C.; Heckmann, A.; Lambert, C. *J. Phys. Chem. C* **2009**, *113*, 2983. (e) Wenger, O. S. *Acc. Chem. Res.* **2011**, *44*, 25. (f) Arrigo, A.; Santoro, A.; Indelli, M. T.; Natali, M.; Scandola, F.; Campagna, S. *Phys. Chem. Chem. Phys.* **2014**, *16*, 818. (g) Natali, M.; Campagna, S.; Scandola, F. *Chem. Soc. Rev.* **2014**, *43*, 4005.

(7) (a) Cias, P.; Slugovc, C.; Gescheidt, G. *J. Phys. Chem. A* **2011**, *115*, 14519. (b) Lambert, C.; Schelter, J.; Fiebig, T.; Mank, D.; Trifonov, A. *J. Am. Chem. Soc.* **2005**, *127*, 10600. (c) Lin, B. C.; Cheng, C. P.; Lao, Z. P. M. *J. Phys. Chem. A* **2003**, *107*, 5241. (d) Malagoli, M.; Bredas, J. L. *Chem. Phys. Lett.* **2000**, *327*, 13.

(8) (a) Adiga, S. P.; Shukla, D. *J. Phys. Chem. C* **2010**, *114*, 2751. (b) Geng, Y.; Wu, S. X.; Li, H. B.; Tang, X. D.; Wu, Y.; Su, Z. M.; Liao, Y. *J. Mater. Chem.* **2011**, *21*, 15558.

(9) (a) Yadav, M.; Singh, A. K.; Pandey, D. S. *Organometallics* **2009**, *28*, 4713. (b) Bronner, C.; Veiga, M.; Guenet, A.; De Cola, L.; Hosseini, M. W.; Strassert, C. A.; Baudron, S. A. *Chem.—Eur. J.* **2012**, *18*, 4041. (c) Hanson, K.; Tamayo, A.; Diev, V. V.; Whited, M. T.; Djurovich, P. I.; Thompson, M. E. *Inorg. Chem.* **2010**, *49*, 6077. (d) Gupta, R. K.; Pandey, R.; Sharma, G.; Prasad, R.; Koch, B.; Srikrishna, S.; Li, P. Z.; Xu, Q.; Pandey, D. S. *Inorg. Chem.* **2013**, *52*, 3687. (e) Gupta, R. K.; Sharma, G.; Pandey, R.; Kumar, A.; Koch, B.; Li, P.-Z.; Xu, Q.; Pandey, D. S. *Inorg. Chem.* **2013**, *52*, 13984. (f) Paitandi, R. P.; Gupta, R. K.; Singh, R. S.; Sharma, G.; Koch, B.; Pandey, D. S. *Eur. J. Med. Chem.* **2014**, *84*, 17. (g) Yadav, M.; Singh, A. K.; Pandey, D. S. *J. Organomet. Chem.* **2011**, *696*, 758. (h) Bronner, C.; Baudron, S. A.; Hosseini, M. W. *Inorg. Chem.* **2010**, *49*, 8659. (i) Klein, J. H.; Sunderland, T. L.; Kaufmann, C.; Holzapfel, M.; Schmiedel, A.; Lambert, C. *Phys. Chem. Chem. Phys.* **2013**, *15*, 16024.

(10) It should be noted, however, that a too strong reduction in the rate of charge recombination can be counter-productive (cf. the behavior of triad **2**). The optimum charge recombination rate for detecting spin effects should match the rate of spin dynamics.

(11) (a) Colvin, M. T.; Ricks, A. B.; Scott, A. M.; Smeigh, A. L.; Carmieli, R.; Miura, T.; Wasielewski, M. R. *J. Am. Chem. Soc.* **2011**, *133*, 1240. (b) Dance, Z. E. X.; Mi, Q. X.; McCamant, D. W.; Ahrens, M. J.; Ratner, M. A.; Wasielewski, M. R. *J. Phys. Chem. B* **2006**, *110*, 25163. (c) Lukas, A. S.; Bushard, P. J.; Weiss, E. A.; Wasielewski, M. R. *J. Am. Chem. Soc.* **2003**, *125*, 3921. (d) Weiss, E. A.; Chernick, E. T.;

DOI: 10.1021/jacs.5b04868
J. Am. Chem. Soc. 2015, 137, 11011−11021

Wasielewski, M. R. *J. Am. Chem. Soc.* **2004**, *126*, 2326. (e) Weiss, E. A.; Ratner, M. A.; Wasielewski, M. R. *J. Phys. Chem. A* **2003**, *107*, 3639. (f) Weiss, E. A.; Tauber, M. J.; Ratner, M. A.; Wasielewski, M. R. *J. Am. Chem. Soc.* **2005**, *127*, 6052. (g) Weiss, E. A.; Ahrens, M. J.; Sinks, L. E.; Gusev, A. V.; Ratner, M. A.; Wasielewski, M. R. *J. Am. Chem. Soc.* **2004**, *126*, 5577.

(12) (a) Salikhov, K. M.; Molin, Y. N.; Sagdeev, R. Z.; Buchachenko, A. L. *Spin polarization and magnetic effects in radical reactions*; Elsevier: Amsterdam, 1984. (b) Steiner, U. E.; Ulrich, T. *Chem. Rev.* **1989**, *89*, 51. (c) Steiner, U. E.; Wolff, H. J. Magnetic Field Effects in Photochemistry In *Photochemistry and Photophysics*; Rabek, J. J., Scott, G. W., Eds.; CRC Press: Boca Raton, FL, 1991; Vol. *IV*, p 1. (d) Hayashi, H. *Introduction to Dynamic Spin Chemistry*; World Scientific Publishing: Singapore, 2004; Vol. *8*.

(13) (a) Desai, P.; Shakya, P.; Kreouzis, T.; Gillin, W. P. *J. Appl. Phys.* **2007**, *102*, 073710. (b) Goto, Y.; Noguchi, T.; Takeuchi, U.; Hatabayashi, K.; Hirose, Y.; Uchida, T.; Sasaki, T.; Hasegawa, T.; Shimada, T. *Org. Electron.* **2010**, *11*, 1212. (c) Ehrenfreund, E.; Vardeny, Z. V. *Isr. J. Chem.* **2012**, *52*, 552. (d) Wang, J. P.; Chepelianskii, A.; Gao, F.; Greenham, N. C. *Nat. Commun.* **2012**, *3*, 1191.

(14) (a) Hanna, M. C.; Nozik, A. J. *J. Appl. Phys.* **2006**, *100*, 074510. (b) Smith, M. B.; Michl, J. *Chem. Rev.* **2010**, *110*, 6891. (c) Jadhav, P. J.; Mohanty, A.; Sussman, J.; Lee, J.; Baldo, M. A. *Nano Lett.* **2011**, *11*, 1495. (d) Ehrler, B.; Walker, B. J.; Bohm, M. L.; Wilson, M. W. B.; Vaynzof, Y.; Friend, R. H.; Greenham, N. C. *Nat. Commun.* **2012**, *3*, 1019. (e) Smith, M. B.; Michl, J. *Annu. Rev. Phys. Chem.* **2013**, *64*, 361. (f) Wilson, M. W. B.; Rao, A.; Ehrler, B.; Friends, R. H. *Acc. Chem. Res.* **2013**, *46*, 1330.

(15) Céspedes-Camacho, I. F.; Matysik, J. Spin in photosynthetic electron transport. In *The Biophysics of Photosynthesis*; Golbeck, J. H., Van der Est, A., Eds.; Springer: New York, 2014; p 141.

(16) (a) Grissom, C. B. *Chem. Rev.* **1995**, *95*, 3. (b) Hore, P. J. *Proc. Natl. Acad. Sci. U. S. A.* **2012**, *109*, 1357. (c) Lambert, N.; Chen, Y. N.; Cheng, Y. C.; Li, C. M.; Chen, G. Y.; Nori, F. *Nat. Phys.* **2013**, *9*, 10.

(17) (a) Ritz, T.; Adem, S.; Schulten, K. *Biophys. J.* **2000**, *78*, 707. (b) Rodgers, C. T.; Hore, P. J. *Proc. Natl. Acad. Sci. U. S. A.* **2009**, *106*, 353. (c) Dodson, C. A.; Hore, P. J.; Wallace, M. I. *Trends Biochem. Sci.* **2013**, *38*, 435.

(18) (a) Werner, U.; Sakaguchi, Y.; Hayashi, H.; Nohya, G.; Yoneshima, R.; Nakajima, S.; Osuka, A. *J. Phys. Chem.* **1995**, *99*, 13930. (b) Kuciauskas, D.; Liddell, P. A.; Moore, A. L.; Moore, T. A.; Gust, D. *J. Am. Chem. Soc.* **1998**, *120*, 10880. (c) Klumpp, T.; Linsenmann, M.; Larson, S. L.; Limoges, B. R.; Burssner, D.; Krissinel, E. B.; Elliott, C. M.; Steiner, U. E. *J. Am. Chem. Soc.* **1999**, *121*, 1076. (d) Mori, Y.; Sakaguchi, Y.; Hayashi, H. *J. Phys. Chem. A* **2002**, *106*, 4453. (e) Rawls, M. T.; Kollmannsberger, G.; Elliott, C. M.; Steiner, U. E. *J. Phys. Chem. A* **2007**, *111*, 3485. (f) Maeda, K.; Henbest, K. B.; Cintolesi, F.; Kuprov, I.; Rodgers, C. T.; Liddell, P. A.; Gust, D.; Timmel, C. R.; Hore, P. J. *Nature* **2008**, *453*, 387. (g) Maeda, K.; Wedge, C. J.; Storey, J. G.; Henbest, K. B.; Liddell, P. A.; Kodis, G.; Gust, D.; Hore, P. J.; Timmel, C. R. *Chem. Commun.* **2011**, *47*, 6563.

(19) Weller, A.; Staerk, H.; Treichel, R. *Faraday Discuss.* **1984**, *78*, 271.

(20) Staerk, H.; Kühnle, W.; Treichel, R.; Weller, A. *Chem. Phys. Lett.* **1985**, *118*, 19.

(21) (a) Cai, J.; Guerreschi, G.; Briegel, H. J. *Phys. Rev. Lett.* **2010**, *104*, 220502. (b) Gauger, E. M.; Rieper, E.; Morton, J. J. L.; Benjamin, S. C.; Vedral, V. *Phys. Rev. Lett.* **2011**, *106*, 040503.

(22) Jones, J. A.; Hore, P. J. *Chem. Phys. Lett.* **2010**, *488*, 90.

(23) (a) Closs, G. L.; Doubleday, C. E. *J. Am. Chem. Soc.* **1973**, *95*, 2735. (b) Haberkorn, R.; Michel-Beyerle, M. E. *Biophys. J.* **1979**, *26*, 489. (c) Schulten, K.; Weller, A. *Biophys. J.* **1978**, *24*, 295. (d) Weller, A. *Z. Phys. Chem. Neue Fol.* **1982**, *130*, 129. (e) Hoff, A. J. *Q. Rev. Biophys.* **1981**, *14*, 599. (f) Brocklehurst, B. *Chem. Soc. Rev.* **2002**, *31*, 301.

(24) Banci, L.; Bertini, L.; Luchinat, C. *Nuclear and Electron Relaxation*; VCH: Weinheim, 1991.

(25) Lüders, K.; Salikhov, K. M. *Chem. Phys.* **1987**, *117*, 113.

(26) Lewis, A. M.; Manolopoulos, D. E.; Hore, P. J. *J. Chem. Phys.* **2014**, *141*, 044111.

(27) Hayashi, H.; Nagakura, S. *Bull. Chem. Soc. Jpn.* **1984**, *57*, 322.

(28) If intermolecular spin−dipolar interactions between the radicals can be neglected, i.e., if the interactions mixing the spin levels are purely local interactions in the two radicals, the couplings between S and $T_{\pm}$ and between T_0 and $T_{\pm}$ are of the same magnitude, differing only in sign.

(29) (a) Bhosale, S. V.; Jani, C. H.; Langford, S. J. *Chem. Soc. Rev.* **2008**, *37*, 331. (b) Andric, G.; Boas, J. F.; Bond, A. M.; Fallon, G. D.; Ghiggino, K. P.; Hogan, C. F.; Hutchison, J. A.; Lee, M. A. P.; Langford, S. J.; Pilbrow, J. R.; Troup, G. J.; Woodward, C. P. *Aust. J. Chem.* **2004**, *57*, 1011. (c) Barros, T. C.; Brochsztain, S.; Toscano, V. G.; Berci, P.; Politi, M. J. *J. Photochem. Photobiol. A-Chem.* **1997**, *111*, 97.

(30) Amthor, S.; Noller, B.; Lambert, C. *Chem. Phys.* **2005**, *316*, 141.

(31) Geiss, B.; Lambert, C. *Chem. Commun.* **2009**, 1670.

(32) (a) Bullock, J. E.; Vagnini, M. T.; Ramanan, C.; Co, D. T.; Wilson, T. M.; Dicke, J. W.; Marks, T. J.; Wasielewski, M. R. *J. Phys. Chem. B* **2010**, *114*, 1794. (b) Gawrys, P.; Djurado, D.; Rimarcik, J. R.; Kornet, A.; Boudinet, D.; Verilhac, J. M.; Lukes, V.; Wielgus, I.; Zagorska, M.; Pron, A. *J. Phys. Chem. B* **2010**, *114*, 1803.

(33) The order of magnitude of electron dipolar interaction is given by $g^2\beta^2/r^3$ At a distance of 20 Å, this corresponds to an equivalent hyperfine field of 0.23 mT. However, the dipolar interaction is fully anisotropic and averaged to zero by molecular rotation.

(34) A similar set of equations has been set up by Werner et al.[18a] According to their definition, $[T_{\pm}] = [T_{+}] = [T_{-}]$. It should be noted that a factor of 2 before k_3 in the bracket factor before [S] is missing in the first line of eq 3.

(35) (a) Schulten, K.; Wolynes, P. G. *J. Chem. Phys.* **1978**, *68*, 3292. (b) Knapp, E. W.; Schulten, K. *J. Chem. Phys.* **1979**, *71*, 1878.

(36) Reszka, K. J.; Takayama, M.; Sik, R. H.; Chignell, C. F.; Saito, I. *Photochem. Photobiol.* **2005**, *81*, 573.

(37) Hötzer, K. A.; Klingert, A.; Klumpp, T.; Krissinel, E.; Bürßner, D.; Steiner, U. E. *J. Phys. Chem. A* **2002**, *106*, 2207.

(38) Gilch, P.; Pollinger-Dammer, F.; Musewald, C.; Michel-Beyerle, M. E.; Steiner, U. E. *Science* **1998**, *281*, 982.

(39) Carrington, A. A.; McLachlan, A. D. *Introduction to magnetic resonance*; Harper and Row: New York, 1967.

(40) Weller, A.; Nolting, F.; Staerk, H. *Chem. Phys. Lett.* **1983**, *96*, 24.

(41) (a) Justinek, M.; Grampp, G.; Landgraf, S.; Hore, P. J.; Lukzen, N. N. *J. Am. Chem. Soc.* **2004**, *126*, 5635. (b) Grampp, G.; Hore, P. J.; Justinek, M.; Landgraf, S.; Lukzen, N. N. *Res. Chem. Intermed.* **2005**, *31*, 567.

(42) Mladenova, B.; Kattnig, D. R.; Kaiser, C.; Schäfer, J.; Lambert, C.; Grampp, G. *J. Phys. Chem. C* **2015**, *119*, 8547.

(43) Lambert, C.; Wagener, R.; Klein, J. H.; Grelaud, G.; Moos, M.; Schmiedel, A.; Holzapfel, M.; Bruhn, T. *Chem. Commun.* **2014**, *50*, 11350.

(44) Mailer, C.; Nielsen, R. D.; Robinson, B. H. *J. Phys. Chem. A* **2005**, *109*, 4049.

(45) Rawls, M. T.; Kuprov, I.; Elliott, C. M.; Steiner, U. E. Spin Relaxation in Ru-Chromophore-Linked Azine/Diquat Radical Pairs. In *Carbon-Centered Free Radicals and Radical Cations*; Forbes, M. D. E., Ed.; John Wiley & Sons: Hoboken, NJ, 2010.

(46) (a) Meyer, V.; Eaton, S. S.; Eaton, G. R. *Appl. Magn. Reson.* **2014**, *45*, 993. (b) Yong, L.; Harbridge, J.; Quine, R. W.; Rinard, G. A.; Eaton, S. S.; Eaton, G. R.; Mailer, C.; Barth, E.; Halpern, H. J. *J. Magn. Reson.* **2001**, *152*, 156.

(47) (a) Solovo'yov, I. A.; Ritz, T.; Schulten, K.; Hore, P. J. A chemical compass for bird navigation. In *Quantum effects in biology*; Mohseni, M., Omar, Y., Engel, G., Plenio, M. B., Eds.; Cambridge University Press: Cambridge, U.K., 2014. (b) Ritz, T.; Wiltschko, R.; Hore, P. J.; Rodgers, C. T.; Stapput, K.; Thalau, P.; Timmel, C. R.; Wiltschko, W. *Biophys. J.* **2009**, *96*, 3451. (c) Hogben, H. J.; Efimova, O.; Wagner-Rundell, N.; Timmel, C. R.; Hore, P. J. *Chem. Phys. Lett.* **2009**, *480*, 118. (d) Efimova, O.; Hore, P. J. *Biophys. J.* **2008**, *94*, 1565. (e) Cintolesi, F.; Ritz, T.; Kay, C. W. M.; Timmel, C. R.; Hore, P. J. *Chem. Phys.* **2003**, *294*, 385.

NOTE ADDED AFTER ASAP PUBLICATION

Equations 7, 9, and 13 were corrected on July 7, 2015. Figure 10 caption was corrected on July 27, 2015.

DOI: 10.1021/jacs.5b04868
J. Am. Chem. Soc. 2015, 137, 11011−11021